International Journal of Advanced Technology and Engineering Exploration, Vol 9(89)
ISSN (Print): 2394-5443 ISSN (Online): 2394-7454
http://dx.doi.org/10.19101/IJATEE.2021.875445

Research Article

An investigation of the ripple reduction capacity of compensated direct torque control with duty ratio optimization for permanent magnet synchronous motor drive

Berhanu Deggefa Lemma* **and Srinivasan Pradabane**
Department of Electrical Engineering, National Institute of Technology Warangal, India

Received: 13-January-2022; Revised: 17-April-2022; Accepted: 19-April-2022

Abstract
The performance of control algorithms is evaluated in both dynamic and steady-state conditions. Direct torque control (DTC) is the ideal option for situations that demand quick dynamics. Despite having the best dynamic response, conventional direct torque control (CDTC) has poor ripple and harmonic performance. The compensated direct torque control with duty ratio optimization (DTC-DRO) is proposed in this work to solve the shortcomings of CDTC. The other four control algorithms were applied to the identical case and their performance was compared to that of DTC-DRO to compare and contrast the ripple and harmonic reduction capabilities of DTC-DRO. For comparison purposes, current control (CC), CDTC, proportional-integral flux manipulated direct torque control (PIFM-DTC), and space vector pulse width modulation (SVPWM) were used. The comparison was made by taking key factors like the torque ripple performance, speed response performance, flux magnitude variation, stator current total harmonic distortion, and voltage total harmonic distortion. To simulate and compare the performance of each control strategy, the Matlab Simulink 2021b environment was utilized. The result of the simulation indicates that all DTC category methods have fast dynamic performance. But the performance of DTC-DRO is better than SVPWM in terms of dynamic and steady-state performance for the considered case. The voltage harmonic distortion, current harmonic distortion, and torque ripple performance of a DTC-DRO are better than those of all control techniques studied in this work. In general, DTC-DRO is suitable for a drive application where fast dynamics and less ripple are required.

Keywords
Compensation, Current control, Conventional DTC, PI flux manipulated DTC, Duty ratio optimized -DTC, Ripple, harmonic, Space vector pulse width modulation.

1.Introduction
Though permanent magnet synchronous motors (PMSMs) have gained widespread popularity due to their high performance, they also have an unwelcome side effect in the form of cogging torque and ripple. Because of these problems, researchers focused on improving control algorithms and motor design for PMSM [1−5]. In some research, a simple control technique was recommended because of its simplicity and fast dynamics [6, 7]. Being simple, the current control (CC) algorithms suffer from variable switching, disturbance, and noise.

To overcome this issue, the social ski-diver-based sunflower optimization approach using an artificial neuro-fuzzy inference system was applied in [8].

Even though optimization and additional features are added to the CC to get better dynamics, the CC has no direct control over the flux. For PMSM, the direct control over a flux has a great effect to run a motor at a variable range. Besides the simplicity of algorithms and signal computation, dynamics and steady-state responses have a great deal to do with the nature of an application. Space vector pulse width modulation (SVPWM) with symmetrical switching and reduced commutation can reduce ripple magnitude. Although SVPWM has many important features, such as power density, ripple performance, and steady-state performance, switching signal generation becomes challenging at multiple levels. Among the existing simple control algorithms, direct torque control (DTC) has a fast dynamic response and direct control over a flux which enhances the control algorithm to be applied to a variable speed operation.

*Author for correspondence

Nowadays, electric drives have become one of the current areas of research interest. From low home consumption equipment for high power applications, the issues related to control and performance improvement have a lot to do with the type of application. The control scheme that produces a high oscillation and ripple has a direct effect on the reliability of the motor [9]. DTC control has fast dynamic performance. Adding the features of duty ratio and torque compensation gives the best dynamic and steady-state performance. The nature of PMSM makes it well suited for field weakening operations compared to other control techniques. When this nature of PMSM is combined with the DTC, it becomes the best option for field weakening regions [10].

The main objective of this work is to investigate the ripple minimization capacity of compensated direct torque control with duty ratio optimization (DTC-DRO) for PMSM drive. To perform these tasks, the combined effect of error compensation and duty ratio optimization based on torque error minimization is applied to control the PMSM drive. To check the control performance of the proposed system, four different controls were compared with the DTC-DRO. These control techniques are CC, SVPWM, conventional direct torque control (CDTC), and proportional-integral flux manipulated direct torque control (PIFM-DTC).

Despite the improved ripple performance, torque oscillation remains between the lower limit and reference torque with the duty ratio optimized DTC. This work includes the use of enhanced DTC with duty ratio and error compensation for PMSM control. Several important parameters were used in this study to assess the performance of the DTC-DRO control technique for PMSM compared to CC, CDTC, PIFM-DTC and SVPWM controlled PMSM drives.

This work is organized as follows: In section two, a literature review is presented. The third section explains the study's methodology, while the fourth section presents the results. The conclusion, discussion, and future work are presented in sections five and six.

2.Literature review

The torque dynamic response of PMSM is directly related to the current angle, which is obtained by omitting the null voltage. DTC has an important feature that suits variable frequency drive because of its capacity to control torque and flux directly. Even though DTC has the best dynamic response, the ripple due to fixed voltage vector switching throughout the switching period is very high. Space vector modulation-based direct torque control (DTC-SVM) was proposed to overcome the drawbacks of CDTC [11]. In DTC-SVM, the change in torque and flux are used to get the reference voltage. The switching signal generation was performed using the reference voltage space vector. Compared to CDTC, this scheme has a little ripple, but the signal computation is more. In addition, the switching signal generation depends on the volt-second balance rather than ripple reduction. The direct flux control capability of DTC makes it preferable for filed weakening applications. For the field weakening region operation, the field magnitude needs to be varied according to the required speed. A good response requires fine control of the programmed flux magnitude. Torque error-related control of flux fluctuation is implemented by adding one proportional-integral controller on CDTC. The proportional integral (PI) control and torque error are utilized to manage the stator flux phase angle to reduce flux ripple in PIFM-DTC. Reduction of the flux ripple plays a great role in determining the range of variable speed. The active voltage is applied to the entire period in CDTC. The use of global optimization to enhance torque performance PMSM was presented in [12]. In this work, the square root of the sum of the average error square is minimized to get the optimal duty. In this scheme, the global optimum duty is obtained, but the limitation of this work is the magnitude of torque is forced to remain between the lower boundary limit and reference torque. Commutation number minimization was proposed to reduce the ripple in [13]. According to this work, an appropriate vector selection was used to reduce the number of commutations. This scheme reduces the ripple as the number of commutation reductions has a significant impact on the ripple. But the drawback of this scheme is that it did not consider the effect of the on-time range of active voltage on ripple. In [14], a fuzzy logic-controlled direct-axis current was proposed to reduce ripple for PMSM drive. Direct axis current (Id) control has a more significant impact on speed than torque ripple. In addition, fuzzy systems use the span to perform a decision. This affects the steady-state and ripple performance. In [15], torque ripple minimization using similarity relations was forwarded for the PMSM drive. In this scheme, the magnitude of error and duty ratio are based on linear relations. Based on the calculated error, the duty ratio is varied between zero and one. The advantage of this scheme is that

duty ratio determination is very simple, but the duty ratio obtained by this method is not the optimal one. Speed, torque, and total harmonic distortion performance enhancement of DTC controlled PMSM was performed by a speed controller tuning using numerical analysis in [16]. The speed controller constant was determined analytically from the motor model. The drawback of this method is that there is no duty ratio manipulation and error compensation. A fixed control set prediction was proposed to minimize torque ripple by considering torque error, the optimal current generation, and the current range limit [17]. In comparison to CDTC, this scheme reduces ripple well, but it requires more computation. Additionally, torque ripple remains between the lower limit and the reference. Duty ratio and voltage phase determination based on error magnitude to get simultaneous improved steady-state and transient performance was proposed in [18]. For small deviation, the computation was performed considering zero error, whereas for large deviation the computation was performed to get fast dynamics. The drawback of this scheme is that it has more computation and one-sided oscillation. In [19], the optimized pulse width modulation ripple minimization technique was proposed. In this control scheme, two active voltages and one null voltage were applied to get the required performance. In this scheme, three switching period spans needed to be calculated. The calculation of the time range for both the active voltage and the null voltage period span needs solving of the simultaneous equations, and this adds more computation. Furthermore, the ripple range in this system changes between the lower limit and the reference value. Sector segmentation was proposed in [20] for improving PMSM performance. In this scheme, the voltage space was segmented into nineteen active voltage states. Based on the reference voltage angle, the switching states were selected. This scheme eliminates the need for hysteresis control. But the drawback of this scheme is that active voltage was applied throughout the switching period. The cogging torque happens due to the nature of PMSM. This component of torque contributes a lot to the production of torque and speed ripple. In [21], the virtual cogging torque was used to minimize the speed ripple by producing an anti-cogging torque that nullifies the effect of the cogging torque produced by PMSM. In this scheme, the effect of the switching time range of active voltage is not taken into account. The efficiency of a motor depends upon the magnitude of harmonic current that contributes to the loss. Harmonic minimization was proposed to improve the efficiency of PMSM [22]. The reduction in harmonic was achieved by applying an appropriate voltage vector. In [23], the efficiency improvement of PMSM analysis was performed considering, copper loss, iron loss, harmonic and flux saturation. In [24], the duty ratio based on speed, flux, torque, and voltage selected for each switching period was used to reduce the torque ripple. The advantage of this scheme is that it considers the speed, magnitude when determining the duty ratio. The ripple level is different for different speed ranges. Duty ratio optimized direct torque control based on torque error root mean square minimization was investigated for dynamic and steady-state enhancement of PMSM drive performance [25]. Even though this scheme is effective in reducing torque, the torque oscillation remains one-sided. In [26], the duty ratio based on the rate of deviation of current was suggested to minimize torque and flux ripple for the DTC. This scheme was effective in reducing both torque and flux ripple, but the parameter range remains between the lower limit and the reference value. Torque and speed manipulated duty ratio was proposed in [27]. If both axis inductances are equal, the only quadrature axis voltage is responsible for compensating the change in torque and counter voltage. Mid-point saturation and extended vector evaluation was used to vary the duty ratio to reduce the torque ripple, but the drawback of these methods is that they do not give an optimal duty ratio [28, 29]. In [30], the duty ratio optimization-based average error minimization was performed. In [31], a duty ratio regulator which takes the effect of speed on torque error was proposed. Based on the speed range, different voltage vectors were applied to control the error in the required range. Twelve merged vectors are applied to reduce the ripple and harmonic, which is the main problem when PMSM is controlled by the DTC algorithm. In the classical duty ratio, the magnitude of the duty ratio depends on machine parameters. The effect of speed on the duty ratio optimization was examined in [32]. This improves duty ratio optimization even more. The duty ratio, which is determined by the minimization of the root mean square of both flux and torque was proposed in [33]. By incorporating the generation of optimal current, in [34], the enhancement was added to the traditional duty ratio computation. The weighting function was employed to enhance response performance. Although the duty ratio optimized DTC has improved ripple performance, torque oscillation remains between the lower limit and reference torque. In [35], the duty ratio optimized model current-predictive was proposed for five-phase PMSM. In this scheme two

drawbacks are there; these are computation numbers and one-sided ripple oscillation of torque. In [36], increasing the number of voltage vectors was proposed as the way to address the torque ripple problem. But again, this scheme increases the commutation number. In general, the duty ratio proposed in the papers reviewed in this work mainly focuses on duty ratio determination. Some of the duty ratio determinations proposed in reviewed papers suggest non-optimal duty ratio estimation The DTC-DRO investigated in this paper combines the advantage of duty ratio and error compensation to effectively reduce the ripple. Several significant parameters were used to evaluate the suggested optimized duty ratio-based DTC-DRO control technique for PMSM with existing control algorithms in this study. Comparisons were made between DTC-DRO, CC, CDTC, PIFM-DTC, and SVPWM controlled PMSM drives. In addition, the DTC-DRO was tested for variable speed to check the effectiveness of the control scheme.

3.Methods

3.1Mathematical dynamic model of PMSM

In the mathematical model, the electromagnetic and mechanical models of PMSM were represented by the equations shown below. Equations 1 to Equation 6, represent the electromagnetic model of PMSM. Equation 7, shows the mechanical model of the machine. Equation 8, links mechanical speed with electrical speed and Equation 9 is used to obtain an electrical angle from synchronous speed.

When the variables used in these equations are defined as below:

V_q= quadrature axis voltage (V)
R= resistance in (ohm)
i_q= quadrature axis current (A)
ψ_q= quadrature axis flux (wb)
ψ_d= direct axis flux (wb)
ω_s= synchronous speed (rad/s)
V_d= direct axis voltage (V)
i_d= direct axis current (A)
L_q= quadrature axis inductance (H)
L_d= direct axis inductance (H)
mf = permanent magnet flux (wb)
P_n= number of poles
Te = electromagnet torque (Nm)
ω_r= rotor speed (rad/s)
B = friction coefficient ($\frac{N.m.s}{rad}$)
J = inertial constant ($\frac{N.m.s^2}{rad}$)
T_L= load torque (Nm)
θ_r= rotor angle (rad/s)
$iabc$=Three-phasecurrent
$i\alpha$ = alpha axis current (A)
$i\beta$ = beta axis current (A).

A. An electromagnetic dynamic model of PMSM

$$V_q = R \times i_q + \frac{d}{dt}(\psi_q) + \omega_s \times \psi d \quad (1)$$

$$i_q = \frac{1}{L_q}\int (V_q - R \times i_q - \omega_s \times \psi_d)dt \quad (2)$$

$$V_d = R \times i_d + \frac{d}{dt}(\psi d) - \omega_s \times \psi_q \quad (3)$$

$$i_d = \frac{1}{L_d}\int (V_d - R \times i_d + \omega_s \times \psi q)dt \quad (4)$$

$$\begin{cases} \psi d = L_d \times i_d + m_f \\ \psi q = Lq \times iq \end{cases} \quad (5)$$

$$T_e = \frac{3}{2} \times P_n(\psi d \times i_q - \psi q \times id) \quad (6)$$

B. Mechanical part

$$J\frac{d}{dt}(\omega_r) = T_e - T_L - B \times \omega_r \quad (7)$$

$$\omega_s = \frac{p_n}{2} \times \omega_r \quad (8)$$

$$\theta_r = \int (\omega_s)\mathrm{dt} \quad (9)$$

C. Coordinate transformation

The conversion between the dq-axis to abc and the dq-axis to αβ is performed by using Equations 10, and Equation 11 respectively.

$$i_{abc} = \begin{bmatrix} cos(\theta_r) & -sin(\theta_r) \\ cos(\theta_r - \frac{2\Pi}{3}) & -sin(\theta_r - \frac{2\Pi}{3}) \\ cos(\theta_r + \frac{2\Pi}{3}) & -sin(\theta_r + \frac{2\Pi}{3}) \end{bmatrix} i_{dq} \quad (10)$$

$$i\alpha\beta = \begin{bmatrix} cos(\theta_r) & -sin(\theta_r) \\ sin(\theta_r) & cos(\theta_r) \end{bmatrix} idq \quad (11)$$

3.2The material used and general layout of DTC-DRO

The ripple minimization capability of a DTC-DRO is explored in this paper by comparing it to simple CC, CDTC, PIFM-DTC, and SVPWM control approach. A constant speed of 50 rad/second and a load torque of 5 Nm are used in the simulation to compare the performance of DTC-DRO with other control schemes. The harmonic component is computed for one cycle, starting at 0.1 seconds. In addition, to show the performance of DTC-DRO over variable speed, the reference speed is varied from 30 rad/s to 45 rad/s and 45 rad/s to 50 rad/s in the time sequence of 0.24 seconds and 0.36 seconds respectively. The harmonic for voltage, current, and flux were measured ta 0.1 seconds, 0.3 seconds, and 0.4 seconds for the speed of 30 rad/s, 45 rad/s, and 50 rad/s speed range respectively. All parameters of the motor, the inverter, and the constant used for simulation purposes are attached to the *Appendix (I and II)*. The general layout of DTC-DRO was

represented by the block diagram as shown in *Figure 1*. The block consists of error compensation, duty ratio determination, switching signal generation, inverter, and PMSM motor.

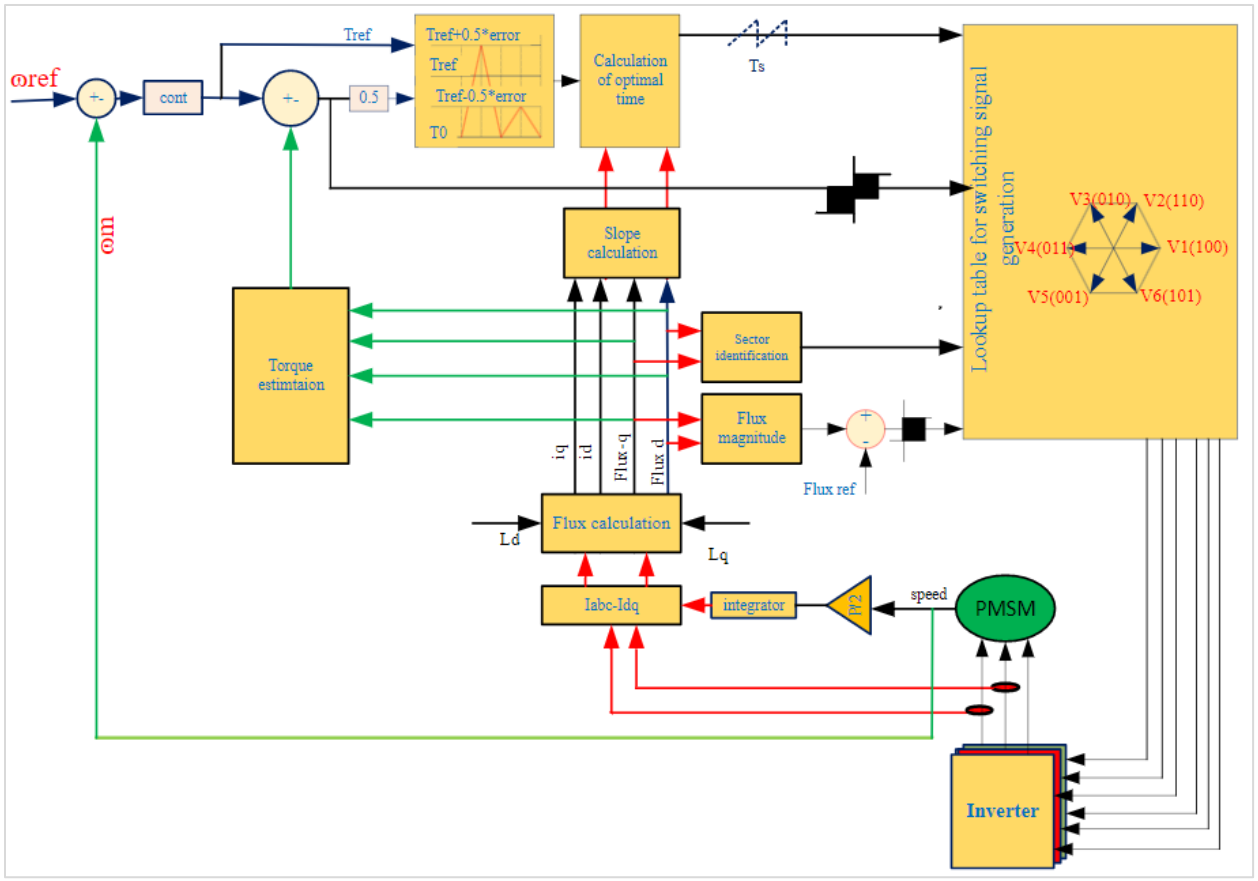

Figure 1 General layout of DTC-DRO

3.2.1Duty ration determination

The slope determination is done by taking the derivative of Equation 6 to a time. Depending on the time range, the slope is different for a time when active voltage is applied and the null voltage is applied. The slope of electromagnetic torque can be defined using Equation 12.

$$\frac{dTe}{dt} = 1.5 \times Pn\left[\frac{d\psi d}{dt} \times iq + \frac{diq}{dt} \times \psi d - \frac{d\psi q}{dt} \times id - \frac{did}{dt} \times \psi q\right] \quad (12)$$

The slope is obtained by substituting equations for id,iq,$\psi q$and ψd. The active voltage period slope is obtained by considering voltage, whereas the null voltage period slope is obtained by substituting zero for Vd and Vq. When the variables V_q, R, i_q, ψ_q,ψ_d, ω_s, V_d, i_d, L_q, L_d, mf , P_n , andTe represent the parameters defined in section 3.1. By substituting the equivalent representation for variables in Equation 12, the expression for active voltage period slope and null voltage period slope were obtained as shown in Equation 13 and Equation 14 respectively. When $S1$represents active voltage period slope, and $S0$ represents null voltage period slope.

$$S1 = 1.5 \times Pn\left[\begin{array}{l} \frac{d(L_d \times i_d + m_f)}{dt} \times \left(\frac{1}{L_q}\int (V_q - R \times i_q - \omega_s \times \psi_d)dt\right) + \\ \frac{d\left(\frac{1}{Lq}\int (V_q - R \times i_q - \omega_s \times \psi_d)dt\right)}{dt} \times (L_d \times i_d + m_f) \\ -\frac{d(Lq \times iq)}{dt} \times \left(\frac{1}{L_d}\int (V_d - R \times i_d + \omega_s \times \psi q)dt\right) \\ -\frac{d\left(\frac{1}{L_d}\int (V_d - R \times i_d + \omega_s \times \psi q)dt\right)}{dt} \times (Lq \times iq) \end{array}\right] \quad (13)$$

The null voltage period slope is obtained by substituting zero for Vd and Vq.

$$S0 = 1.5 \times Pn\begin{bmatrix} \frac{d(L_d \times i_d + m_f)}{dt} \times (\frac{1}{L_q}\int(-R \times i_q - \omega_s \times \psi_d)dt) + \\ \frac{d(\frac{1}{L_q}\int(-R \times i_q - \omega_s \times \psi_d)dt)}{dt} \times (L_d \times i_d + m_f) \\ -\frac{d(Lq \times iq)}{dt} \times (\frac{1}{L_d}\int(-R \times i_d + \omega_s \times \psi q)dt) \\ -\frac{d(\frac{1}{L_d}\int(-R \times i_d + \omega_s \times \psi q)dt)}{dt} \times (Lq \times iq) \end{bmatrix} \quad (14)$$

Based on the slope, the torque developed by the motor when active voltage is applied for an active period and the remaining time is covered by null voltage can be written as shown in Equation 15. when variables used in Equation 15 to Equation 18 are defined as shown below.

Tsp = optimal switching period
$T0$ = torque at the starting of the switching period
$u(t)$ = unit step function
t = time
Ts = switching time
$Tref$ = reference torque
$Trefm$ = reference modified torque
$error$=the difference between reference and developed torque

$$Te = \begin{cases} T0 + S1 \times t, When\ t < Tsp \\ (T0 + S1 \times Tsp) \times u(t - Tsp) + S0 \times u(t - Tsp) \times (t - Tsp), When\ t > Tsp \end{cases} \quad (15)$$

By minimizing, the root means square error between torque and the reference torque the optimal time is achieved.

$$\frac{d}{dT_{sp}}\sqrt{\frac{1}{Ts}\left(\int_0^{Ts}(Tref - Te)^2\, dt\right)} = 0 \quad (16)$$

By solving for the variable, the following equation was obtained for the optimal switching time.

$$Tsp = \frac{Tref - T0}{S1 - S0} + \frac{S0 \times Ts}{S1 - S0} \quad (17)$$

The torque reference can be compensated such that the developed torque will oscillate around both sides of the required torque. The newly defined reference torque is represented by the equation below, where Trefm is the new reference value of torque, Tref is the reference torque, and error is the difference between developed torque and the reference torque.

$$Trefm = Tref + 0.5 \times \text{sign}(error) \times |error| \quad (18)$$

3.2.2Voltage vector selection

For CDTC and PIFM-DTC, only three inputs are used for signal generation. But for DTC-DRO fourth input is added. The fourth input is the optimal switching period. The optimal time is used to decide the active voltage time. *Figure 2*, indicates the voltage selection strategy used for this work. Switching state variables in *Figure 2* are defined as under.

$\Delta\Psi^{\uparrow}$ = positive flux error,
$\Delta T^{\uparrow}$= positive torque error,
n= sector number
$\Delta\Psi^{\downarrow}$= negative flux error,
$\Delta T^{\downarrow}$= negative torque error,
V= voltage vector state

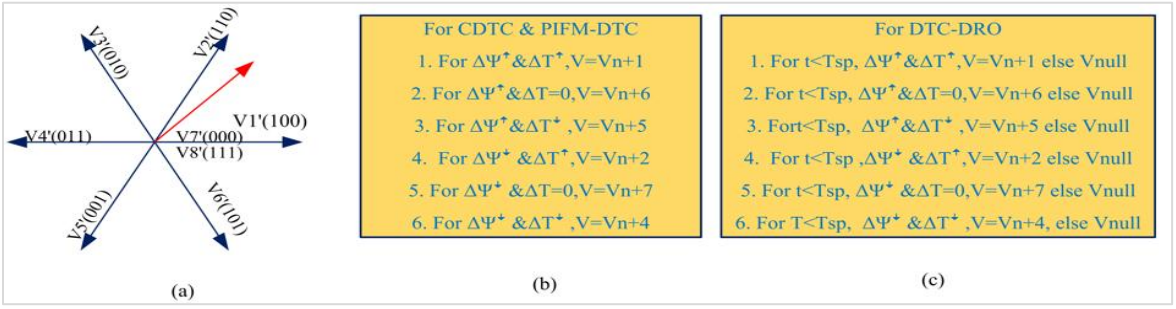

Figure 2 Voltage selection strategy, when (a) shows the voltage vector status, (b) shows the voltage selection strategy for CDTC and PIFM-DTC, and (c) shows the voltage selection method for DTC-DRO

4.Simulation result

The simulation was performed in Matlab 2021b. The mathematical models of PMSM, inverter and signal processing were developed in the Simulink environment. The signal processing includes coordinate transformation, flux computation, torque estimation, slope determination, and error compensation. From the slope, the initial torque at the start of the switching time, and modified reference torque, the duty ratio was determined. From the duty ratio, flux hysteresis controller output, torque hysteresis controller output, and sector number, the lookup table was used to generate the

switching signal. The simulation was performed considering two cases. The two cases were constant speed and variable speed operation. The constant speed operation was performed to compare the DTC-DRO with other control schemes. Whereas the variables the variable speed was done to indicate the suitability of DTC-DRO for the variable operation of PMSM drive.

Current control

The current control (CC) of PMSM is a street forward control that has no algorithm complexity. The simple schematic for signal generation of current is depicted below, when the inverter, motor, and sensing circuit are the same as that of the DTC-DRO shown above in *Figure 1*. The reference current generation requires a simple manipulation of the reference torque obtained from the speed controller.

A simple method of generating the switching signal for CC is illustrated in *Figure 3*. A reference torque is generated from the speed error controller and used to calculate a reference current. The electromagnetic torque formula is changed to the Equation 19 when the magnitude of the q-axis and d-axis inductance is equal.

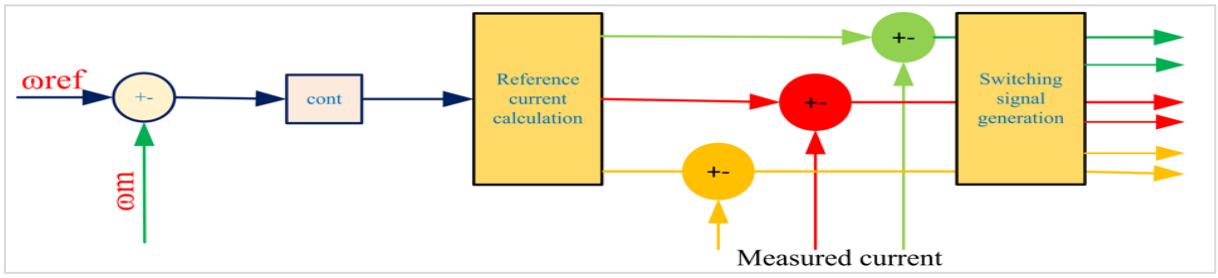

Figure 3 Schematic diagram of current control signal generation

$$Tref = 1.5 \times P_n(mf \times i_{qref}) \quad (19)$$

The magnitude of the q-axis current is obtained from the maximum current by $Iref * sin(\theta r)$ when $\theta r$the is current angle (Equation 20). The reference current is obtained by Equation 21, when Tref is the reference torque from the speed controller, mf is permanent magnet flux, and P_n is the pole of the motor.

$$Iref = \frac{Tref}{1.5 \times mf \times Pn} \quad (20)$$

For a constant zero magnitude of d-axis reference current, the three-phase current reference is obtained by using the equation shown below.

$$iabs_{ref} = I \times \begin{bmatrix} sin(\theta r + \pi/2) \\ sin(\theta r - \pi/6 \\ sin(\theta r + 7 * \pi/6) \end{bmatrix} \quad (21)$$

By comparing the reference to a stator motor current, the switching signals are obtained. The difference between the stator measured current and reference current obtained from Equation 21, is supplied to the hysteresis controller. Based on the magnitude of error, the output is generated for triggering the switch. Negation is used to generate a gating signal for the switch on the same leg of an inverter. *Figure 4*, shows the simulation result of the current controlled PMSM.

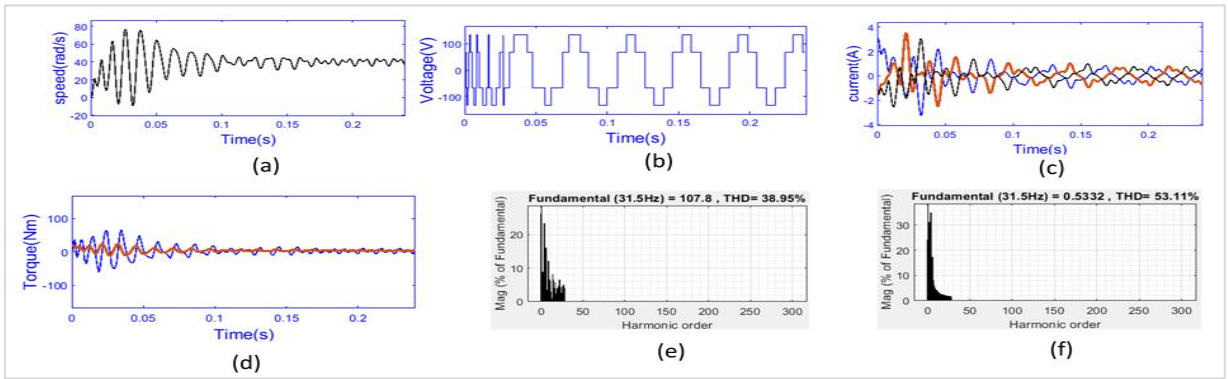

Figure 4 (a) Speed (b) Voltage waveform (c) Current waveform (d) Torque response (e) Voltage harmonic (f) Current harmonic

Conventional DTC

Both current and voltage harmonic distortion are high for the current-controlled variable frequency drive. Another control technique praised for the simplicity of an algorithm and for giving a fast dynamic response is direct torque control. To generate a switching signal, the simple conventional direct torque control uses a torque error, flux error, and sector number. The sector number is obtained from the estimated flux angle. In *Figure 5*, there are three inputs for switching signal generation. These inputs are obtained from torque error, flux error, and angle of flux. The torque difference is calculated by taking the difference of speed controller output and estimated torque by Equation 6. Flux error is calculated by taking the difference between reference flux and estimated flux. The estimated flux is calculated from machine parameters and operating current using Equation 5. The third input sector number is obtained from the angle of the estimated flux. The sector identification has two-step, angle calculation, and sector number assignment. The angle is obtained by taking the inverse tan of the ratio of Ψq to Ψd. Based on the magnitude of this ratio the sector number is obtained.

The logic for sector identification is for CDTC and PIFM-DTC:

If the ratio is between 0 to 60 the sector number is 1

else if the ratio is between 60 to 120 the sector number is 2

else if the ratio is between 120 to 180 the sector number is 3

else if the ratio is between 180 to 240 the sector number is 4

else if the ratio is between 240 to 300 the sector number is 5

else if the ratio is between 300 to 360 the sector number is 6

once sector number, torque error, and flux error are obtained, the voltage vectors selection is performed based on the criteria depicted in *Figure 2 (b).*

The result of the simulation shown in *Figure 6* indicates the torque and speed response at constant torque of 5 Nm and 50 rad/s. The simulation indicates the flux ripple, voltage harmonics, current harmonics, and flux harmonic for CDTC of PMSM.

Proportional-integral flux manipulated DTC (PIFM-DTC)

The modified flux angle is determined by adding the torque error controller's output to the flux angle, according to the PIFM-DTC. This scheme is implemented by following the step explained for CDTC, except for the flux angle manipulation based on torque error magnitude and sign. Having all similarities PIFM-DTC differs from CDTC by angle manipulation. For PIFM-DTC like that of CDTC, the torque difference is calculated by taking the difference of speed controller output and estimated torque by Equation 6. The angle is obtained as the sum of the angle calculated from the inverse tan of the ratio of Ψq to Ψd and torque error controller output. This step is shown in *Figure 7* and in Equation 22. Except for this modification, the switching signal generation, and vector selection are similar to that of CDTC.

The flux angle is obtained by Equation 22 when the variables are defined as follows:

θnew = new flux angle

ki = integral constant

θf = flux angle

kp = proportional constant

$$\theta new = \theta f + (k_p + \frac{k_i}{s}) \times (Tref - Te) \qquad (22)$$

The same principle of switching signal generation and sector identification is used in PIFM-DTC, except for the angle modification based on torque error.

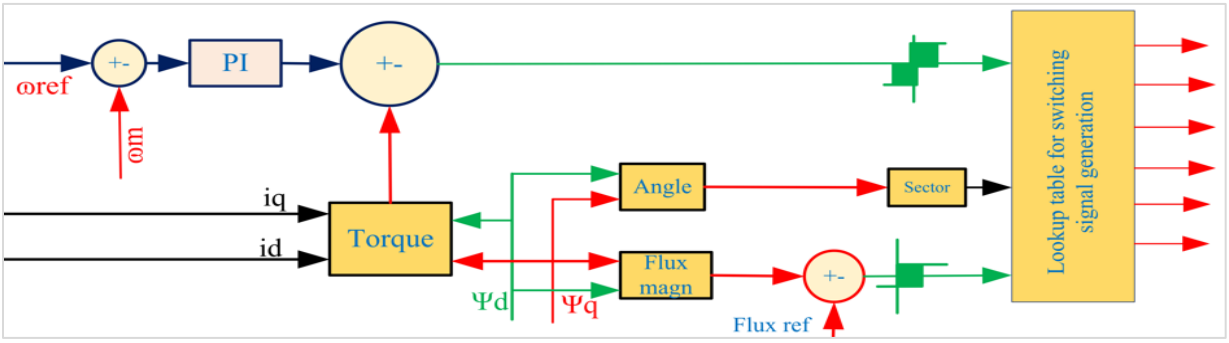

Figure 5 Schematics diagram of CDTC

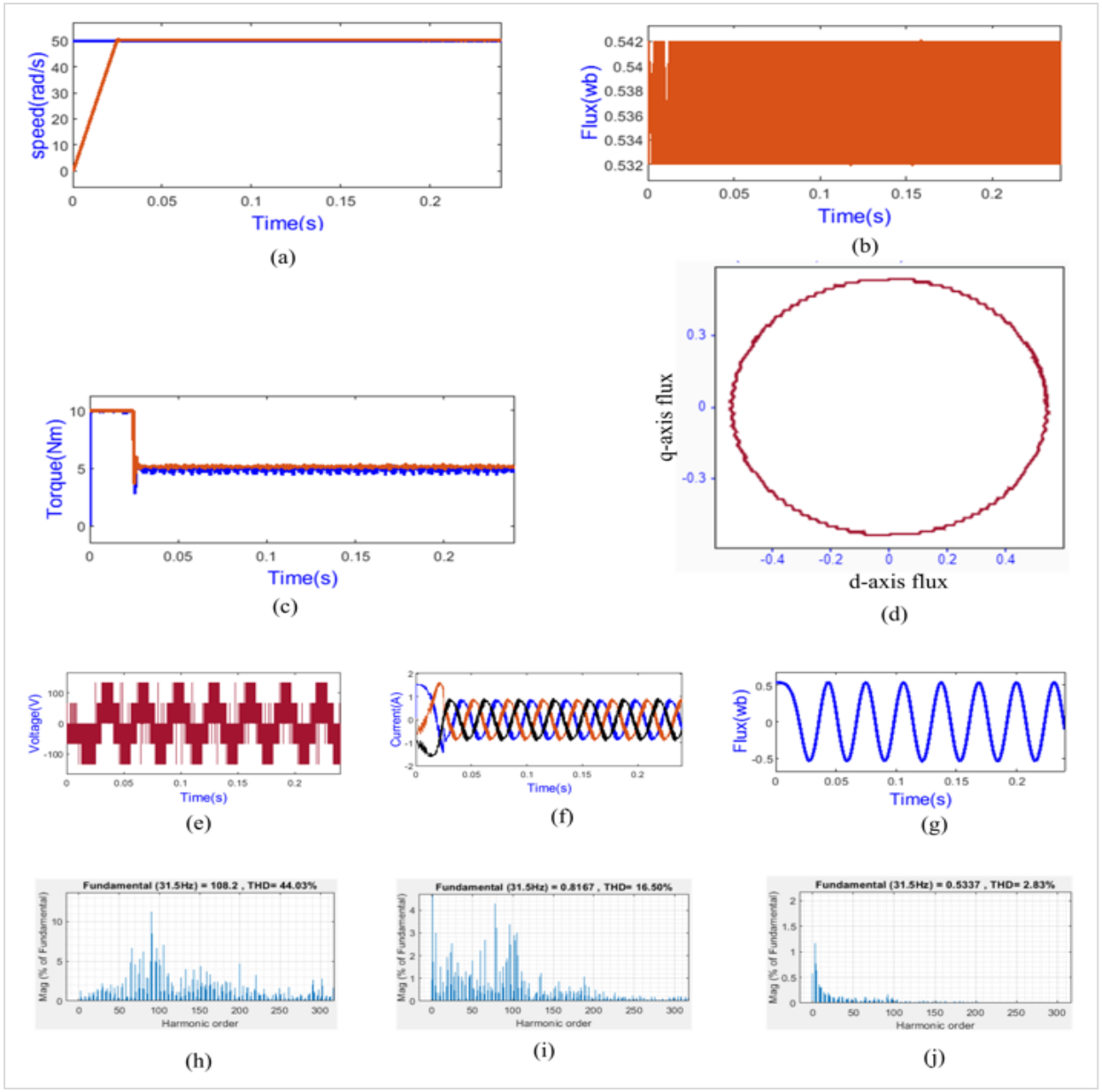

Figure 6 Simulation result for CDTC of PMSM when (a) Speed response (b) Flux variation (c) Torque response (d) Flux plot (e) Voltage waveform (f) Current waveform (g) Flux waveform (h) Harmonics of voltage (i) Current harmonics (j) Flux harmonic

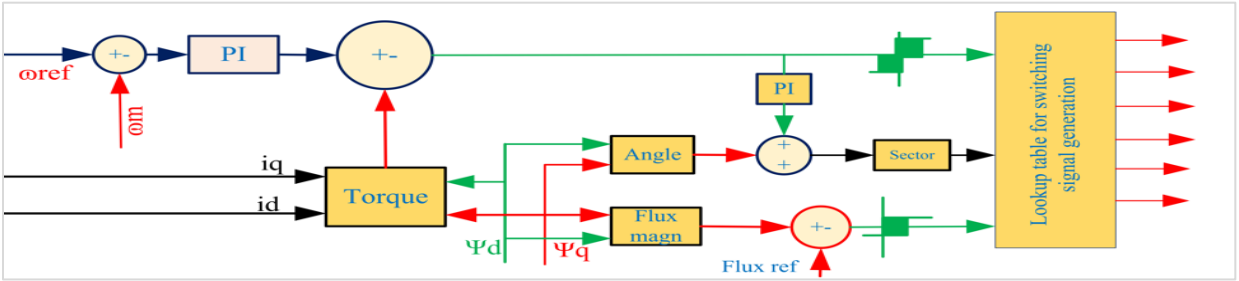

Figure 7 Schematics diagram of flux manipulated DTC (PIFM-DTC)

Torque is produced in large part by the quadrature current component and the d-axis flux. In particular, the quadrature current plays a crucial role. When the torque error is negative, the flux angle decreases, which in turn decreases the flux on the q-axis. If the initial flux is at position b depicted in *Figure 8*, and the torque error is positive, the angle will increase. Simulation results are shown in *Figure 9*. This brings the flux to position b+ and the angle of flux changes from θ2 to θ3. But for the original flux position, if the torque error is negative, the flux position changes from position b to position b-. From this, the magnitude of the q-axis current can be obtained by Equation 23 for positive torque error. The sign of the q-axis current is the same as the sign of torque change. When Δiq = change in q-axis current

$$\Delta iq = \frac{b^{+} - b}{Lq} \qquad (23)$$

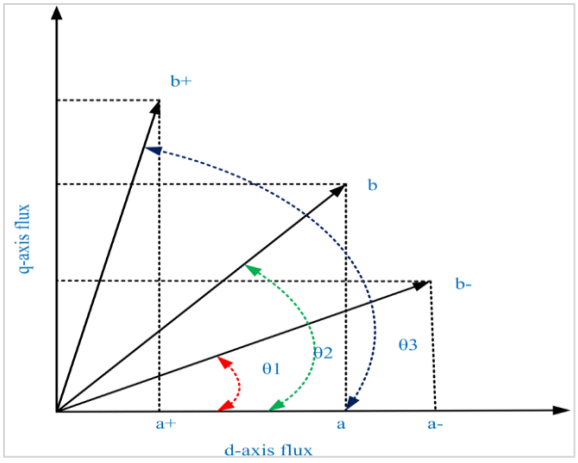

Figure 8 Effect of flux variation on the magnitude of the torque

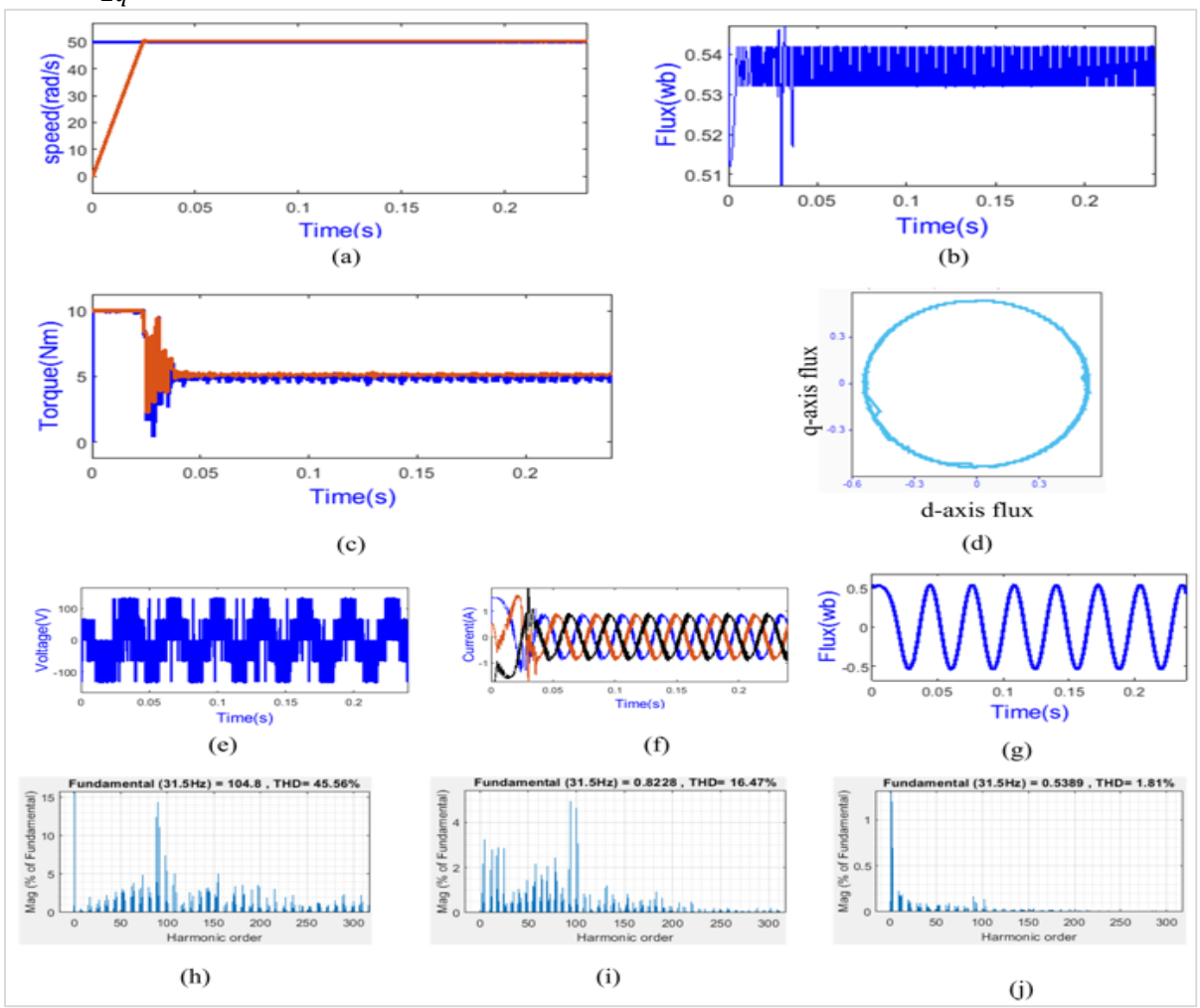

Figure 9 Simulation result for PIFM-DTC of PMSM when (a) Speed response (b) Flux variation (c) Torque response (d) Flux plot (e) Voltage waveform (f) Current waveform (g) Flux waveform (h) Harmonics of voltage (i) Current harmonics (j) Flux harmonic

SVPWM controlled PMSM

SVPWM is an extended sinusoidal pulse width modulation. SVPWM can reduce the ripple, especially when the symmetry of switching time is applied. To reduce ripple, the symmetric pulse width modulation scheme with a minimum switching scheme that reduces the commutation number was applied. For constant $\frac{3*Vref*Ts}{Vdc}$, when $Vref$is the reference voltage, $Ts$is switching time, and $Vdc$is Dc voltage, the dwelling time is obtained by Equation 24. The reference current $iqref$is obtained from the output of the torque controller. The reference torque is obtained from the output of the speed controller whereas the developed torque is obtained by Equation 6. The difference between these torques is supplied to the controller to get $iqref$whereas $idref$ is set to zero. The difference between a reference and a motor current is supplied controller to get the reference voltage. The feedforward is added to decouple the two-axis parameter. Finally, the coordinate transformation is performed to get the reference in the αβ axis. From this reference voltage, the magnitude of the reference voltage and angle were calculated. The angle is obtained by taking the inverse tan of the ratio of $V_{\beta ref}$ to $V_{\alpha ref}$. Based on the magnitude of this ratio the sector number is obtained (*Figure 10*).

The logic for sector identification for SWPWM

If the ratio is between 0 to 60 the sector number is 1

else if the ratio is between 60 to 120 the sector number is 2

else if the ratio is between 120 to 180 the sector number is 3

else if the ratio is between 180 to 240 the sector number is 4

else if the ratio is between 240 to 300 the sector number is 5

else if the ratio is between 300 to 360 the sector number is 6

The sector identification is the same for CDTC, PIFM-DTC, and SVPWM. The only difference is that the angle is obtained from flux for the case of CDTC and PIFM-DTC, but the angle is obtained from the reference voltage for SVPWM.

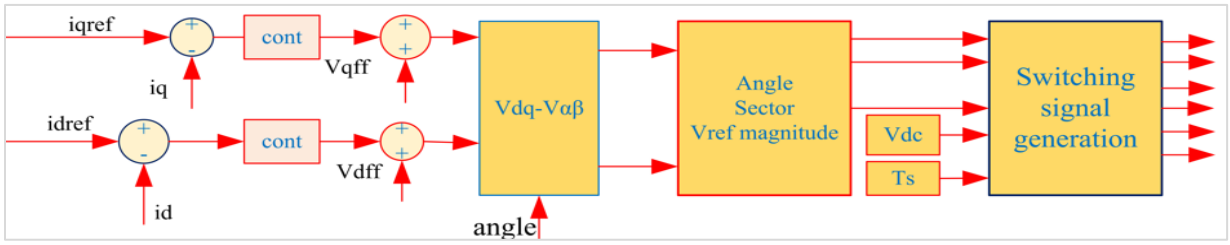

Figure 10 SVPWM control signal generation scheme

From the sector (n), reference voltage angle (α), Vdc, and switching time (Ts) the dwelling time was calculated using Equation 24.

$$\begin{cases} T1 = k * sin(\frac{n*pi}{3} - \alpha) \\ T2 = k * sin(\alpha - (\frac{(n-1)*pi}{3})) \\ T0 = Ts - T1 - T2 \end{cases} \quad (24)$$

Figure 11, shows the simulation result for SVPWM control of PMSM.

Duty ratio optimized DTC (DTC-DRO)

Figure 12, shows the result for DTC-DRO controlled PMSM. Duty ratio optimization is taken as a means to reduce the ripple for DTC-controlled PMSM. Compared to *Figure 4(d)*, *Figure 6(c)*, *Figure 9(c)*, and *Figure 11(d)*, the torque ripple *of Figure 12(c)* is small. In addition, from *Figure 13(b)* and *Figure 13(c)*, it can be seen that the current and voltage harmonics are very small for DTC-DRO.

Performance of DTC-DRO at variable speed

To analyze the performance of the PMSM controlled by DTC-DRO at variable speed and constant torque of 5 Nm, the speed was kept at 30 rad/s up to 0.24 seconds, 45 rad/s from 0.24 seconds to 0.36 seconds, 50 ad/s from 0.36 seconds to 0.5 seconds. The voltage harmonics, current harmonic, flux harmonic, torque ripple, and flux ripple were taken in each span. The simulation results are depicted in *Figure 14*, *Figure 15*, and *Figure 16*. The harmonic is measured in each speed range to analyze the speed performance at a variable range. The total harmonic distortion (THD) was measured for one cycle starting at 0.1 seconds, 0.3 seconds, and 0.4 seconds for the speed range of 30 rad/s, 45 rad/s, and 50 rad/s respectively. As it is shown in *Figure 15*, the voltage harmonics, current harmonics, and flux harmonics are better for the 50 rad/s compared to 30 rad/s and 45 rad/s.

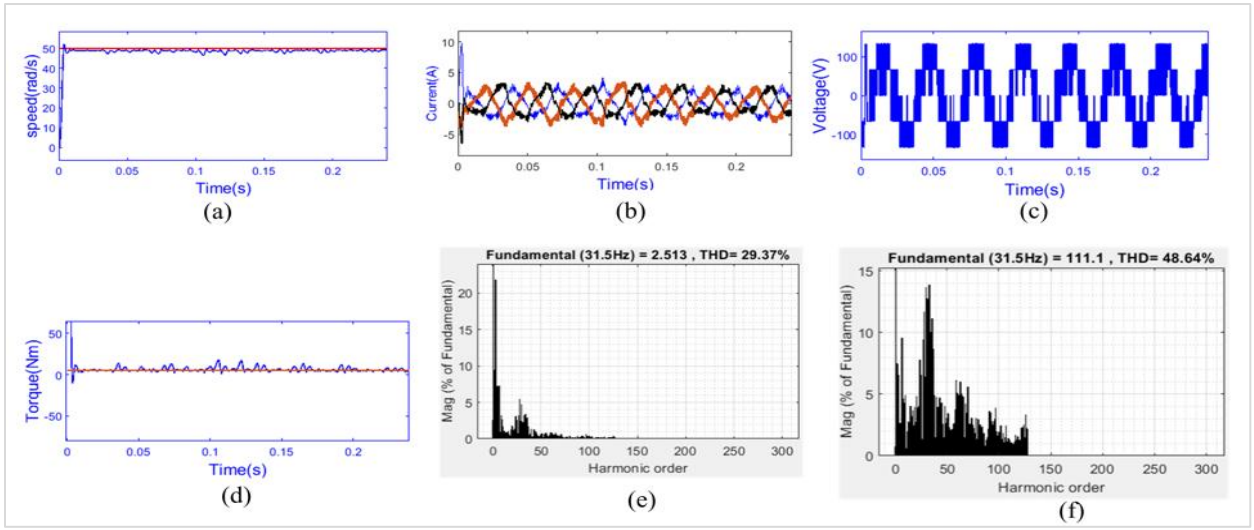

Figure 11 (a) Speed response (b) Torque response (c) Voltage harmonic, and (d) Current harmonic

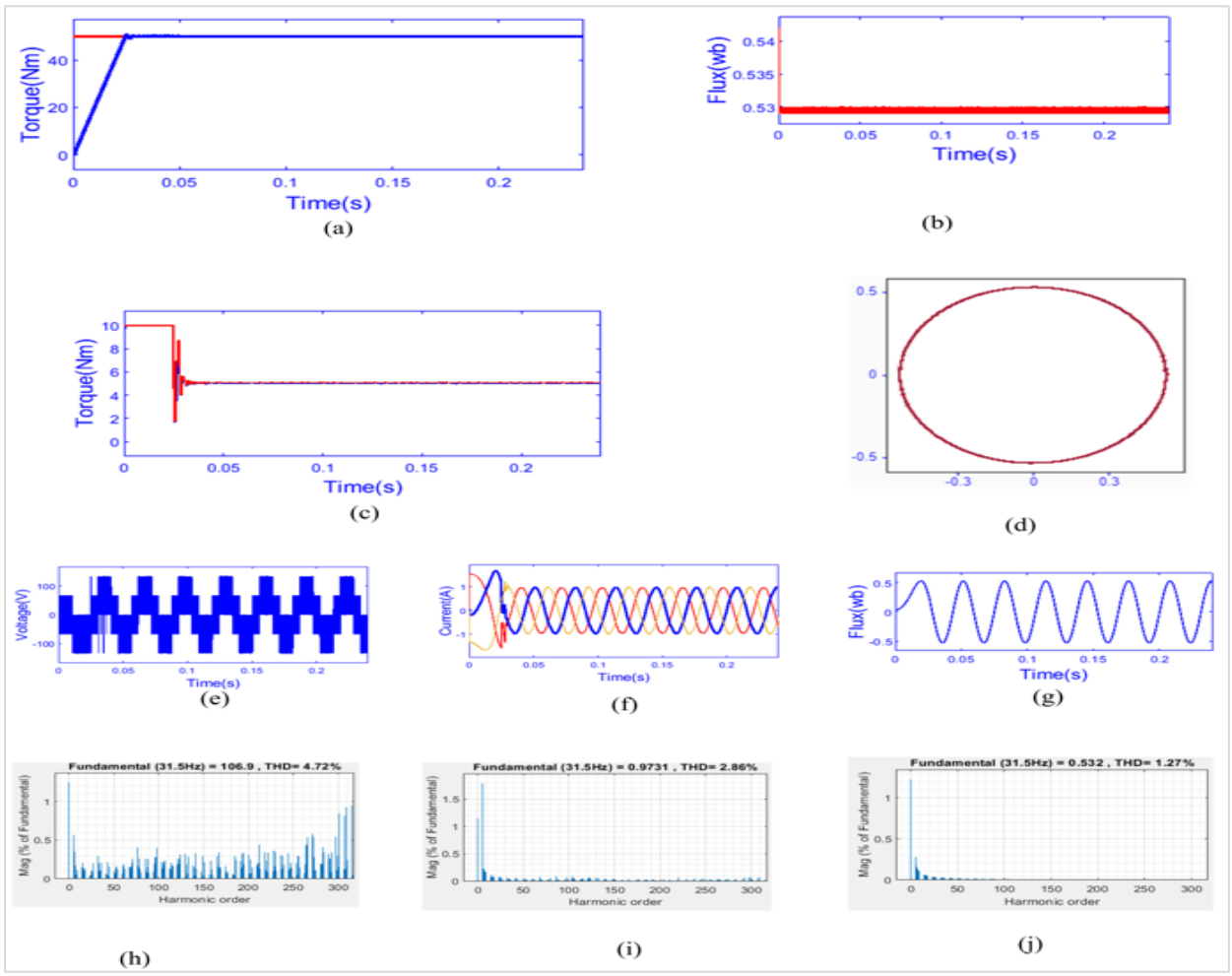

Figure 12 Simulation result for DTC-DRO of PMSM, when (a) Speed response (b) Flux variation (c) Torque response (d) Flux plot (e) Voltage waveform (f) Current waveform (g) Flux waveform (h) Harmonics of voltage (i) Current harmonics (j) Flux harmonic

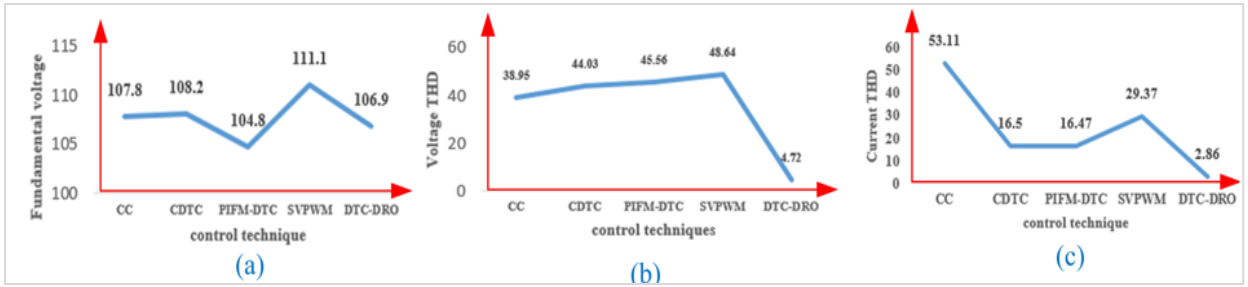

Figure 13 Comparison of control techniques when (a) Fundamental component of voltage, (b) Voltage harmonic, and (c) Current harmonics

In *Figure 14*, the diagram labeled (a) indicates the speed response for the variable speed operation and the diagram labeled (b) indicates the torque response for constant load and variable speed operation. The diagram in *Figure 15*, indicates the voltage harmonics, current harmonics, and flux harmonics at different speed levels. *Figure 15 (a)* indicates the voltage THD, *Figure 15 (b)* indicates current THD whereas *Figure 15 (c)* indicates the flux THD. The plot in *Figure 16*, shows the voltage, current, and flux waveform for variable speed operation with their harmonic. The THD is measured for different speed ranges. The frequency corresponding to the speed range was displayed on the THD plot of voltage, current, and flux.

5.Discussion

The improvement in torque and speed ripple was obtained from two important factors for DTC-DRO. These factors are duty ratio optimization and error compensation. Duty ratio optimization was done to limit active voltage time to reduce the ripple limit. Another factor is error compensation for modification of reference torque to modify the optimal switching period. This modification was performed to divide the one-sided error to both sides of the reference torque. This is performed to reduce the error. In addition to this logic, from the comparative analysis of CC, CDTC, PIFM-DTC, SVPWM, and DTC-DRO, the latter is effective in reducing torque and speed ripple. Simulation results in *Figure 4*, indicate that the current control technique gives a fast dynamic response with a high speed and torque ripple. In addition, it can be seen that the current and voltage total harmonics are high for this control method. The result of the simulation for the CDTC of PMSM in *Figure 6* indicates that the CDTC of PMSM provides nearly similar speed and torque dynamics to the current control. But the magnitude of current and voltage harmonics is better for CDTC compared to current control. The results of the simulation in *Figures 6*, *Figure 8*, and *Figure 12* indicate that the dynamics of motor torque and speed are the same for CDTC, PIFM-DTC, and DTC-DRO. However, DTC-DRO has much smaller ripple magnitudes due to the optimized duty ratio and compensated reference torques. The flux variation range is from 0.532-0.542 for CDTC, 0.535-0.54 for PIFM-DTC, and 0.529-0.530 for DTC-DRO. This indicates that the DTC-DRO has less flux ripple compared to the remaining two DTC categories. The results of the simulation in *Figure 6*, *Figure 8*, and *Figure 12*, also indicate that the plot of flux for DTC-DRO is smoother than in the remaining two cases. This indicates that the DTC has a better capability of controlling the flux. In PIFM-DTC, torque deviation controls the magnitude of flux variation. It can be seen in *Figures 6* and *Figure 9*, that the magnitude of the flux variation for the PIFM-DTC is better than that of the CDTC. In addition, PIFM-DTC's flux plot is smoother than CDTC's.

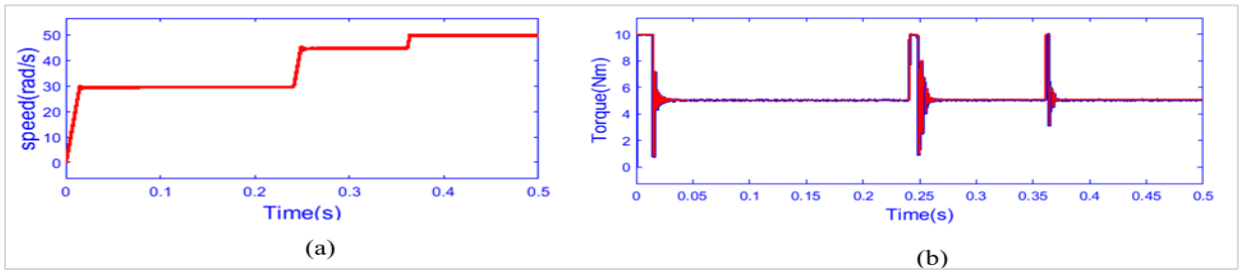

Figure 14 Variable speed response (a) Speed response and (b) Torque response

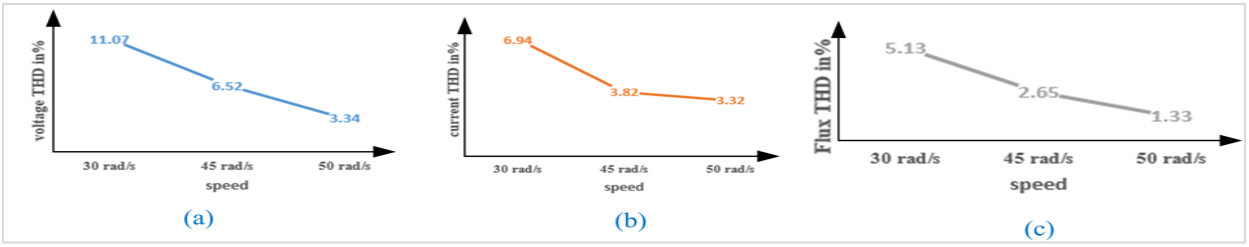

Figure 15 THD of DTC-DRO for variable speed, when (a) is voltage THD, (b) is current THD, (c) is flux THD

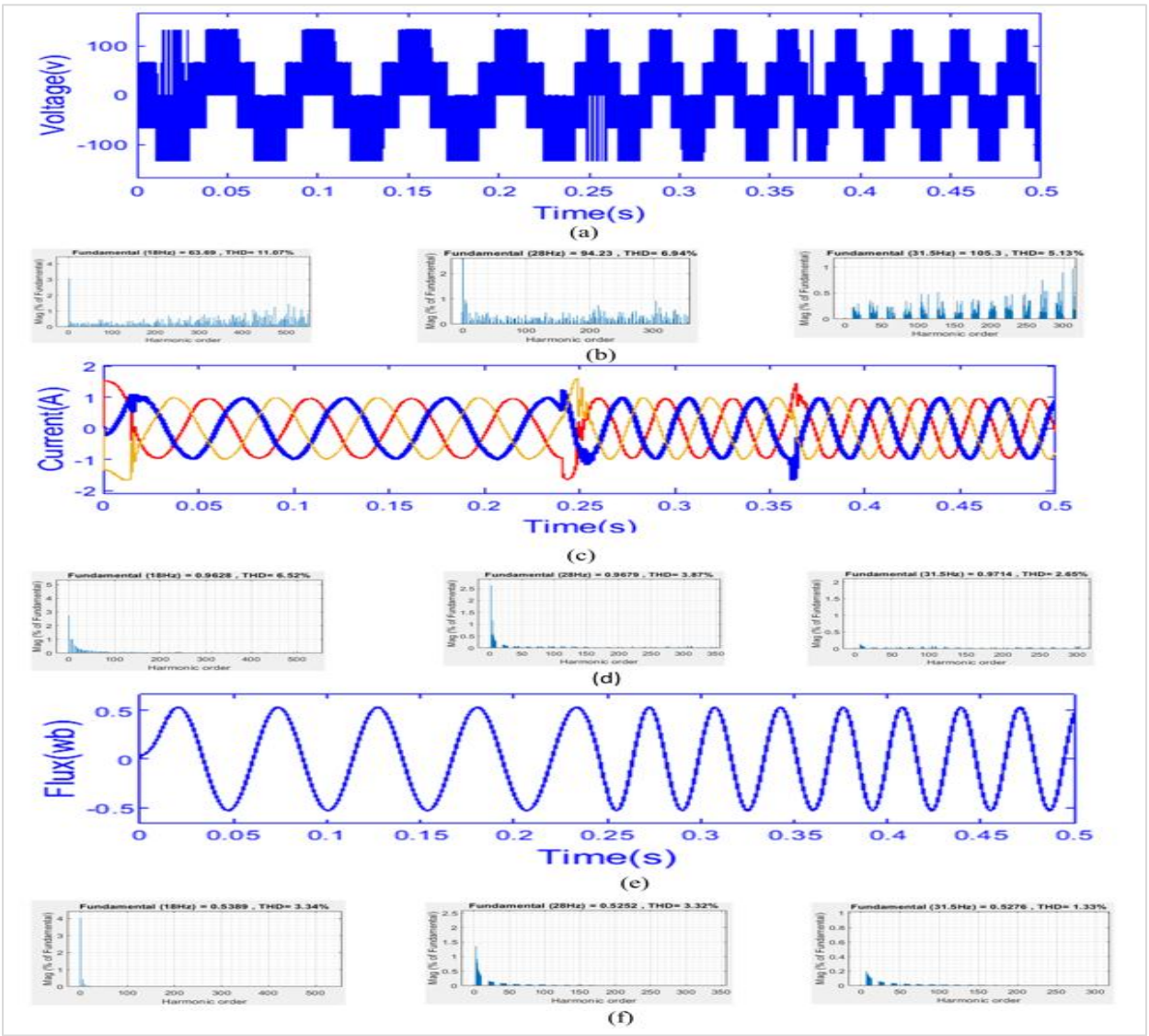

Figure 16 indicate variable speed performance, (a) Voltage waveform (b) Voltage harmonics for 30 rad/s, 45 rad/s and 50 rad/s (c) Current waveform (d) Current harmonic for 30 rad/s, 45 rad/s and 50 rad/s (e) Flux harmonic (f) flux harmonic for 30 rad/s, 45 rad/s and 50 rad/s

SVPWM's harmonic content is nearly identical to the current control harmonic content. However, the fundamental component of the voltage is much higher. DTC-DRO has a very low flux harmonic distortion. In addition, the DTC-DRO performance was tested by varying the speed.

Figure 16, indicates the voltage, current, and flux harmonic is very low for 50 rad/s (480 rpm) compared to low-speed operation. In general, compared to other control schemes used for comparison in this work, DTC-DRO has better performance for both constant speed and variable operation. The key finding of this investigation is that even though the process of duty time computation and torque error computation is added to CDTC, the DTC-DRO is effective in reducing speed and torque ripple. In addition, the harmonic performance of DTC-DRO is better compared to other control schemes presented in this work.

The limitation of the scheme is that although this method combines the simplicity of CDTC, duty ratio minimization for ripple reduction, and error compensation for dividing ripple to both sides of the reference torque, the computations involved for duty ratio determination, error compensation, and adding one input for selection voltage vector add complexity compared to CDTC.

6.Conclusion and future work

The efficacy of direct torque control with duty ratio optimization (DTC-DRO) for PMSM drives to reduce ripple was examined in this study. Voltage THD, current THD, flux ripple, torque ripple, and speed ripple were taken as the key factors for performing the investigation. The result of the simulation indicates that, in terms of all key factors, DRO-DTC has a better performance compared to the control techniques presented in this study. But the SVPWM produces a high magnitude of fundamental voltage magnitude compared to all the techniques studied in this work. So, DTC-DRO is suited for applications where low ripple and fast dynamic responses are required. In the future, this control method will be extended for an open-end winding and multi-phase PMSM.

Acknowledgment

None.

Conflicts of interest

The authors have no conflicts of interest to declare.

Authors' contribution statement

Berhanu Deggefa Lemma: Carried out the literature review of control techniques, modeling, simulation, writing, and preparing the manuscript. **Srinivasan Pradabane:** Revised the manuscript and proofread the article.

References

[1] Bida VM, Samokhvalov DV, Al-mahturi FS. PMSM vector control techniques-a survey. In conference of Russian young researchers in electrical and electronic engineering (EIConRus) 2018 (pp. 577-81). IEEE.

[2] Aydin M, Gulec M. A new coreless axial flux interior permanent magnet synchronous motor with sinusoidal rotor segments. IEEE Transactions on Magnetics. 2016; 52(7):1-4.

[3] Demir Y, Aydin M. A novel dual three-phase permanent magnet synchronous motor with asymmetric stator winding. IEEE Transactions on Magnetics. 2016; 52(7):1-5.

[4] Onsal M, Demir Y, Aydin M. A new nine-phase permanent magnet synchronous motor with consequent pole rotor for high-power traction applications. IEEE Transactions on Magnetics. 2017; 53(11):1-6.

[5] Veena VS, Achari S, Ravichandran MH, Praveen RP. Vector control of three phase PMSM drive using power transformations for future spacecraft application. In international conference on circuits, power and computing technologies 2014 (pp. 313-9). IEEE.

[6] Kumar KR, Nithin K, Kumar TV. Torque ripple reduction in PMSM drive based on instantaneous voltage control technique. In power India international conference 2016 (pp. 1-6). IEEE.

[7] Dobzhanskyi O, Amiri E, Gouws R. Comparison analysis of electric motors with two degrees of mechanical freedom: PM synchronous motor vs induction motor. In international young scientists forum on applied physics and engineering 2016 (pp. 14-7). IEEE.

[8] Mukhopadhyay J, Choudhuri S, Sengupta S. ANFIS based speed and current control with torque ripple minimization using hybrid SSD-SFO for switched reluctance motor. Sustainable Energy Technologies and Assessments. 2022.

[9] Roque JP, Bolam RC, Vagapov Y, Anuchin A. Numerical analysis of an electric high-speed rim-driven rotor. In international workshop on electric drives: advances in power electronics for electric drives 2022 (pp. 1-4). IEEE.

[10] Dianov A. Optimized field-weakening strategy for control of PM synchronous motors. In 29th international workshop on electric drives: advances in power electronics for electric drives 2022 (pp. 1-6). IEEE.

[11] Lemma BD, Pradabane S. Ripple torque lessening in space vector pulse width modulation based direct torque control of permanent magnet synchronous motor drive. In journal of physics: conference series 2021 (pp. 1-7). IOP Publishing.

[12] Shyu KK, Lin JK, Pham VT, Yang MJ, Wang TW. Global minimum torque ripple design for direct torque control of induction motor drives. IEEE Transactions on Industrial Electronics. 2009; 57(9):3148-56.

[13] Zhang Y, Zhu J. Direct torque control of permanent magnet synchronous motor with reduced torque ripple

and commutation frequency. IEEE Transactions on Power Electronics. 2010; 26(1):235-48.
[14] Basit BA, Choi HH, Jung JW. An online torque ripple minimization technique for IPMSM drives: fuzzy system-based d-axis current design approach. IEEE Transactions on Industrial Electronics. 2020; 68(12):11794-805.
[15] Shinohara A, Inoue Y, Morimoto S, Sanada M. Maximum torque per ampere control in stator flux linkage synchronous frame for DTC-based PMSM drives without using q-axis inductance. IEEE Transactions on Industry Applications. 2017; 53(4):3663-71.
[16] Odo K, Ohanu C, Chinaeke-ogbuka I, Ajibo A, Ogbuka C, Ejiogu E. A novel direct torque and flux control of permanent magnet synchronous motor with analytically-tuned PI controllers. International Journal of Power Electronics and Drive Systems. 2021; 12(4):2103-12.
[17] Liu Q, Hameyer K. Torque ripple minimization for direct torque control of PMSM with modified FCSMPC. IEEE Transactions on Industry Applications. 2016; 52(6):4855-64.
[18] Vafaie MH, Dehkordi BM, Moallem P, Kiyoumarsi A. Improving the steady-state and transient-state performances of PMSM through an advanced deadbeat direct torque and flux control system. IEEE Transactions on Power Electronics. 2016; 32(4):2964-75.
[19] Kim SJ, Kim JW, Park BG, Lee DH. A novel predictive direct torque control using an optimized PWM approach. IEEE Transactions on Industry Applications. 2021; 57(3):2537-46.
[20] Wang M, Sun D, Zheng Z, Nian H. A novel lookup table based direct torque control for OW-PMSM drives. IEEE Transactions on Industrial Electronics. 2020; 68(10):10316-20.
[21] Bu F, Yang Z, Gao Y, Pan Z, Pu T, Degano M, et al. Speed ripple reduction of direct-drive PMSM servo system at low-speed operation using virtual cogging torque control method. IEEE Transactions on Industrial Electronics. 2020; 68(1):160-74.
[22] El AA, Hasoun M, Khafallah M, Benkirane K. Efficiency improvement of dual three-phase permanent magnet synchronous motor using modified switching table DTC for electric ship propulsion. International Journal of Power Electronics and Drive Systems. 2021; 12(3):1315-25.
[23] Elsherbiny H, Ahmed MK, Elwany MA. Online efficiency optimization of IPMSM for electric vehicles. International Journal of Power Electronics and Drive Systems. 2021; 12(3):1369-78.
[24] Cheema MA, Fletcher JE, Xiao D, Rahman MF. A direct thrust control scheme for linear permanent magnet synchronous motor based on online duty ratio control. IEEE Transactions on Power Electronics. 2015; 31(6):4416-28.
[25] Vafaie MH, Dehkordi BM, Moallem P, Kiyoumarsi A. A new predictive direct torque control method for improving both steady-state and transient-state operations of the PMSM. IEEE Transactions on Power Electronics. 2015; 31(5):3738-53.
[26] Zhang Z, Liu X. A duty ratio control strategy to reduce both torque and flux ripples of DTC for permanent magnet synchronous machines. IEEE Access. 2019; 7:11820-8.
[27] Niu F, Huang X, Ge L, Zhang J, Wu L, Wang Y, et al. A simple and practical duty cycle modulated direct torque control for permanent magnet synchronous motors. IEEE Transactions on Power Electronics. 2018; 34(2):1572-9.
[28] Zhang Z, Wei C, Qiao W, Qu L. Adaptive saturation controller-based direct torque control for permanent-magnet synchronous machines. IEEE Transactions on Power Electronics. 2015; 31(10):7112-22.
[29] Xia C, Wang S, Gu X, Yan Y, Shi T. Direct torque control for VSI-PMSM using vector evaluation factor table. IEEE Transactions on Industrial Electronics. 2016; 63(7):4571-83.
[30] Niu F, Li K, Wang Y. Direct torque control for permanent-magnet synchronous machines based on duty ratio modulation. IEEE Transactions on Industrial Electronics. 2015; 62(10):6160-70.
[31] Nasr A, Gu C, Wang X, Buticchi G, Bozhko S, Gerada C. Torque-performance improvement for direct torque-controlled PMSM drives based on duty-ratio regulation. IEEE Transactions on Power Electronics. 2021; 37(1):749-60.
[32] Ren Y, Zhu ZQ, Green JE, Li Y, Zhu S, Li Z. Improved duty-ratio-based direct torque control for dual three-phase permanent magnet synchronous machine drives. IEEE Transactions on Industry Applications. 2019; 55(6):5843-53.
[33] Ma C, Yao X, Li H, De BF. An improved two-vector model predictive torque control based on RMS duty ratio optimization for PMSM. In international electric machines & drives conference 2019 (pp. 1674-9). IEEE.
[34] Inoue T, Inoue Y, Morimoto S, Sanada M. Maximum torque per ampere control of a direct torque-controlled PMSM in a stator flux linkage synchronous frame. IEEE Transactions on Industry Applications. 2016; 52(3):2360-7.
[35] Saeed MS, Song W, Yu B, Wu X. Low-complexity deadbeat model predictive current control with duty ratio for five-phase PMSM drives. IEEE Transactions on Power Electronics. 2020; 35(11):12085-99.
[36] Hsu HY, Wu ZX, Hsieh MF. A simplified regulable duty cycle direct torque control method for permanent magnet synchronous motor. In international conference on electrical machines and systems.2021 (pp. 1730-5). IEEE.

Berhanu Deggefa Lemma was born Diksis, Ethiopian in 1988. He received his BSc and M.Sc. from Adama Science and Technology University in 2012 and 2017 respectively. Currently, he is a research scholar at the National Institute of Technology Warangal. He has presented a paper at the international conference. He is working on a PMSM drive.
Email: berhanu@student.nitw.ac.in

Dr. Srinivasan Pradabane was born in Pondicherry, India 1983. He received his graduate degree from the Pondicherry University in 2005 and his post-graduate degree from Anna University in 2008. He received his Ph.D. from NITW in 2016. He did his post-doctoral research in the United Kingdom in 2021. He published many articles in reputable journals. His research interests include Multilevel Inverters; PWM Schemes; Induction Motor Drives; Electric Vehicles; Integration of Renewable, DC Motor Drives, BLDC Drives, PMSM Drives, LIM Drives, Propulsion Technology for Vehicles, Measurement Techniques, Open-End Winding Drives, Driver Circuits and digital control.
Email: spradabane@nitw.ac.in

Appendix I

S. No.	Abbreviation	Description
1	CC	Current Control
2	CDTC	Conventional Direct Torque Control
3	DTC	Direct Torque Control
4	DTC-DRO	Compensated Direct Torque Control with Duty Ratio Optimization
5	DTC-SVM	Space Vector Modulation-Based Direct Torque Control
6	$error$	Shows the Difference Between Reference and Developed Torque
7	Flux ref	Reference Flux
8	Id	Direct Axis Current
9	Iq	Quadrature Axis Current
10	iα	Alpha Axis Current
11	iβ	Beta Axis Current
12	J	Inertial Constant
13	Ki	Integral Constant
14	Kp	Proportional Constant
15	Ld	Direct Axis Inductance
16	Lq	Quadrature Axis Inductance
17	n	Sector Number
18	PI	Proportional Integral
19	PIFM-DTC	Proportional-Integral Flux Manipulated Direct Torque Control
20	PMSM	Permanent Magnet Synchronous Motor
21	SVPWM	Space Vector Pulse Width Modulation
22	THD	Total Harmonic Distortion
23	Tref	Reference Torque
24	Trefm	Modified Reference Torque
25	Ts	Switching Period
26	Tsp	Optimal Switching Period
27	T0	Torque at the Start of the Switching Period
28	u(t)	Unit Step Function
29	V	Voltage Vector State
30	Vd	Direct Axis Voltage
31	Vdc	DC Voltage
32	Vq	Quadrature Axis Voltage
33	Vqff	quadrature Axis Feedforward Voltage
34	Vref	Reference Voltage
35	Ψd	Direct Axis Flux
36	Ψq	Quadrature Axis Flux
37	θr	Rotor Angle
38	ωm	Motor Speed
39	ωr	Rotor Speed
40	ωref	Reference Speed
41	ωs	Synchronous Speed
42	$\Delta\Psi^{\uparrow}$	Positive Flux Error
43	$\Delta\Psi^{\downarrow}$	Negative Flux Error
44	$\Delta T^{\uparrow}$	Positive Torque Error
45	$\Delta T^{\downarrow}$	Negative Torque Error
46	θnew	New Flux Angle
47	θf	Flux Angle
48	Δiq	Change in Quadrature Axis Current

Appendix II

Parameter	Magnitude	Parameter	Magnitude	Parameter	Magnitude
Vdc	200 V	Speed	50 rad/sec	Tl	5 Nm
Ld	21.3 mH	Fs	1 kHz	J	0.0024 Nm.sec2 /rad
Lq	24.2 mH	Ra	0.24 ohm	B	0.001 Nm.se/rad
mf	0.542 wb	Pole	8	IMAX	10 A